A Dual-Signaling Ferrocene-Pyrene Dyad: Triple-Mode Recognition of the Cu(II) Ions in Aqueous Medium

Manzoor Ahmad Wani, Mrituanjay D. Pandey, Rampal Pandey, Sandeep Kumar Maurya & Debabrata Goswami

Journal of Fluorescence

ISSN 1053-0509
Volume 27
Number 6

J Fluoresc (2017) 27:2279-2286
DOI 10.1007/s10895-017-2169-0

Springer

J Fluoresc (2017) 27:2279–2286
DOI 10.1007/s10895-017-2169-0

ORIGINAL ARTICLE

A Dual-Signaling Ferrocene-Pyrene Dyad: Triple-Mode Recognition of the Cu(II) Ions in Aqueous Medium

Manzoor Ahmad Wani[1] · Mrituanjay D. Pandey[1] · Rampal Pandey[1] · Sandeep Kumar Maurya[2] · Debabrata Goswami[2]

Received: 22 June 2017 / Accepted: 10 August 2017 / Published online: 24 August 2017

Abstract We report a structure of ferrocene-pyrene conjugate (**1**) comprising electro and photo-active dual-signaling units. In particular, **1** upon interaction with Cu(II), displays selectively one-photon fluorescence quenching, but it shows two-photon absorption (TPA) cross-section 1230 GM (at 780 nm). Further, **1** displayed two irreversible oxidative waves at 0.39 V and 0.80 V (vs Ag/AgCl), in the electrochemical analysis which upon addition of Cu^{2+}, led to the negative potential shift in both the oxidative waves to appear at 0.25 V and 0.68 V. The triple mode changes in presence of Cu(II) suggesting the possible application of **1** for the detection of Cu(II) in aqueous media.

Keywords Ferrocene · Pyrene · Two-photon absorption · Fluorescence quenching · Electrochemical response

Introduction

Literature reveals that generally change in the optical properties (absorption/emission) upon binding of a metal ion to a ligand can be used as a method for designing new molecules as metal ion selective sensors [1, 2]. Because of the high sensitivity of fluorescence technique even at very low concentrations, fluorescence-based molecular sensors are in applicable vogue in recent past [3–6]. We have been actively working in the area of fluorescent detection of ions for few years [7–11]. Copper is third most abundant and essential element in the human body due to its various elementary physiological course of actions, however excess amount of Cu^{2+} causes severe neurodegenerative disease [12]. Fast and efficient detection of Cu^{2+} in the environment and biology is becoming a major hot topic for chemists [13–17] owing to the problems encountered by Cu^{2+} in the cancer cells wherein its concentration changes remarkably (in serum of the peripheral blood of healthy children and children with acute lymphocytic leukemia ranging to 114–328 μg $dL-1$) [18]. Deficiency of copper in human body can cause hematological symptoms [19] and numerous neurological problems [20]. Chaamni et al. studied the binding effect of various metal ions (Viz. Cu^{2+}) to human serum albumin, human holo-transferrin and human transferring for therapeutic use [21–24].

Of particular interest are the efficient two photon absorbing materials with large two-photon absorption (TPA) cross-sections owing to their extensively explored for various applications [25, 26]. Studies on molecular systems possessing TPA cross sections have revealed that one of its prime contributions is extensive electron delocalization within the molecular framework [27–30]. In accordance with this observation, design of molecular systems for TPA activity has relied on coupling of donor

Electronic supplementary material The online version of this article (doi:10.1007/s10895-017-2169-0) contains supplementary material, which is available to authorized users.

✉ Mrituanjay D. Pandey
mrituanjaypandey@gmail.com

✉ Rampal Pandey
rppandeysu@gmail.com

✉ Debabrata Goswami
dgoswami@iitk.ac.in

[1] Department of Chemistry, Dr. H. S. Gour Central University, Sagar 470003, India

[2] Department of Chemistry, Indian Institute of Technology Kanpur, Kanpur 208016, India

(D) and acceptor (A) units through π-bridges to achieve extensively delocalized/ conjugated structures [31–34]. The TPA cross sections (σ) within such frameworks emerges to increase with the enhanced donor/ acceptor capabilities of the chemical motifs connected to each other as well as with the extent of conjugation between them, along with the overall planarity of the π-bridge [35, 36].

In addition to fluorescence-based methods, recently it is being perceived in view of the fact that metal ion-complexation can lead to dramatic third-order nonlinear optical (NLO) behaviour [37–39]. Therefore, it should be possible to use TPA as a means of selectively detecting metal ions in solution, although such TPA-based selective metal ion sensors are indeed very rare [40–42]. In this context, we have been recently exploring the proper design of ligands which upon binding with metal ion exhibit significant changes in third order NLO activity and TPA so that selective detection could be made possible [43–45]. The electrochemically active ferrocene motif and the photophysically active pyrene motif altogether within the same system have been explored for sensing applications [46–49]. Bures et al. revealed the intramolecular charge-transfer and nonlinear optical properties of the ferrocene-donor and organic-acceptor (D-π-A) systems [50].

With these objectives, we report herein the ferrocenyl-1-pyreneamine conjugate (**1**) as a multichannel sensing system (Fig. 1). Interestingly, **1** exhibits potential to be used for Cu(II) sensor. **1** upon interaction with Cu(II) results fluorescence quenching and TPA activity in aqueous media as a detection response. A negative potential shift in the oxidative wave of **1** has also been observed. Notably, **1** upon interaction with Cu(II) increases TPA significantly which allows a more reliable and positive detection of Cu (II) ion in aqueous media. Structurally similar, ferrocene–pyrene imine dyad has been developed by Singh et al. as a 'turn-on' chemodosimeter for Cr^{3+} in THF-H2O solution [51].

Experimental Section

General Experiment

UV–visible spectra were recorded on a Perkin-Elmer-Lambda 20 UV–vis spectrometer and fluorescence spectra were recorded on a Varian Luminescence Cary eclipsed with a 10 mm quartz cell at 25 °C. Melting points were measured using a JSGW melting point apparatus and are uncorrected. ^{1}H and ^{13}C-NMR spectra were obtained on a JEOL-JNM LAMBDA 400 model spectrometer operating at 400.0 and 100.00 MHz respectively, in $CDCl_3$ solutions. The chemical shifts are referenced with respect to TMS. ESI high resolution mass spectra (ESI-HRMS) were recorded on a MICROMASS QUATTRO II triple quadrupole mass spectrometer. The ESI capillary was set at 3.5 kV and the cone voltage was 40 V. Cyclic voltammetry was performed on a BAS Epsilon electrochemical workstation using a platinum working electrode, an Ag/AgCl reference electrode (3M NaCl) and a platinum-wire counter electrode. The ferrocene/ferrocenium couple was taken as the internal standard with its $E_{1/2} = +0.51(70)$ V (vs Ag/AgCl under the same experimental conditions). The crystal data for the compound **1** were collected on a Bruker SMART APEX CCD Diffractometer. The program SMART (version 6.45) was used for integration of the intensity of reflections and scaling. The program SADABS was used for absorption correction. The crystal structure was solved and refined by full matrix least-squares methods against F^2 by using the program SHELXL-97. All non-hydrogen atoms were refined with anisotropic displacement parameters. Hydrogen positions were fixed at calculated positions and refined isotropically. Crystallographic data and structure refinement details for **1** are given in Table S1. CCDC 820,409 for **1** contains the supplementary crystallographic data for this paper. This data can be obtained free of charge from the Cambridge Crystallographic Data Centre (CCDC) via http://www.ccdc.cam.ac.uk/data_request/cif. 1-Pyrenylamine, ferrocene-2-carboxaldehyde and metal salts such as $Cu(ClO_4)_2 \cdot 6H_2O$, $Pb(ClO_4)_2 \cdot xH_2O$, $Li(ClO_4)$ and $Na(ClO_4) \cdot H_2O$ were

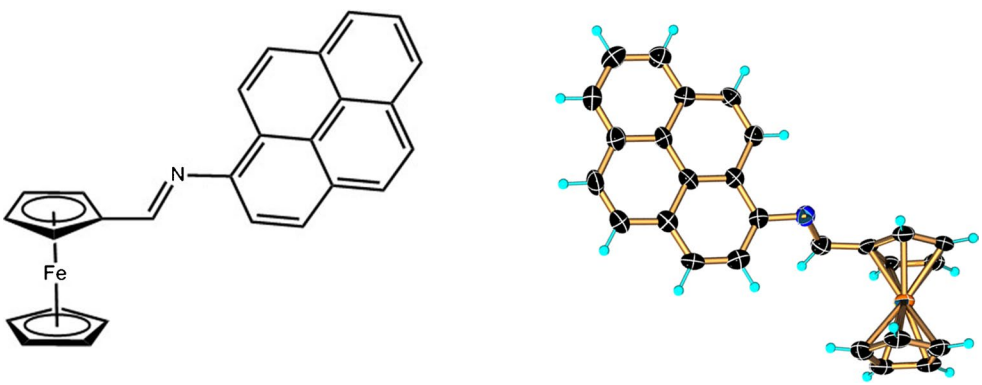

Fig. 1 Structure (left) and ORTEP diagram (right) of **1** with 70% thermal ellipsoid

purchased from Aldrich chemical company (USA) while $Mg(ClO_4)_2{\cdot}6H_2O$, $Ca(ClO_4)_2{\cdot}4H_2O$, $Mn(ClO_4)_2{\cdot}6H_2O$, $Ni(ClO_4)_2{\cdot}6H_2O$, $Zn(ClO_4)_2{\cdot}6H_2O$, $Cd(ClO_4)_2{\cdot}4H_2O$ were prepared from the reaction of their carbonate salts with perchloric acid. Fluorescence quantum yields were determined by comparison with anthracene as a fluorescence standard ($\varphi = 0.27$) [52–58]. Stability constants (K_a) were calculated by following a reported procedure [59].

Two Photon Absorption

The open-aperture (OA) z-scan (intensity scan) method was used for determining the TPA cross-section values of the samples [60]. Femtosecond Mode-locked Ti: Sapphire laser (Model 900) was used for the study of TPA activity which is pumped by a Coherent Verdi frequency doubled Nd: Vanadate laser. Laser system is tunable from 730 nm to 900 nm with the repetition rate of 76 MHz. A mechanical chopper (Model: MC1000A) with a 50% duty cycle was used to employ the blanking in the laser pulse sequence. The optimized chopper frequency of 1 kHz was used to minimize the cumulative thermal effect arising from the sample heating with HRR pulses [61, 62]. Sample solutions are held in a 1 mm quartz cuvette for the OA z-scan experiments. As used in previous experiments [43] a 20 cm lens focused the 160 fs pulses into the sample cell resulting in a focused intensity of ~1 GW/cm^2. Rayleigh range in our set up was 1.3 mm at 770 nm, as the beam waist at the focus was 17 µm. The 1 mm sample cell choice satisfied this Rayleigh range criteria for z-scans. For a smooth OA z-scan, the sample was scanned through the focal point of the lens using a motorized translation stage (Newport Inc. model ESP 300 with a minimum step-size of 0.1 µm) and the transmitted beam was focused with a 7.5 cm focal length lens into a UV-enhanced amplified silicon photodiode detector (Thorlabs DET210). The photodiode voltage was measured using the peak-to-peak mode in an oscilloscope (Tektronix TDS 224 model, digital real time oscilloscope) that was triggered by the chopper frequency. The delay stage and the oscilloscope are interfaced with the computer using a GPIB card (National Instruments Inc.) and the data was acquired using a LabVIEW programming. The resulting data were fitted at different z positions to calculate transmittance (T) with the following equation [63].

$$\beta = 2\sqrt{2}\frac{(1 - T(z))}{I_0 L}\left(1 + \left(\frac{Z}{Z}\right)^2\right)$$

Where all the other parameters are known, β can be calculated easily. Subsequent to obtaining the values of β, the TPA cross-section of the chromophore (σ_2, in units of 1 GM = 10^{-50} cm^4.s/photon.molecule) is generated from the expression: $\sigma_2 = \beta h\nu * 10^3/Nc$, where ν is the frequency of the incident laser beam, N is Avogadro constant, c is the concentration of the chromophore in respective solvents. The σ_2 for Rhodamine-6G in methanol at 806 nm was used as a calibration of our measurement [64, 65].

Synthesis of 1

1-Pyrenylamine (0.214 g, 1.00 mmol) was dissolved in hot methanol (20 mL) and a methanolic solution of ferrocene-2-carboxaldehyde (0.217 g, 1.00 mmol) was added dropwise to it and the resulting solution was further stirred at 50 °C for 8 h. A reddish precipitate obtained was filtered, washed with hot methanol and recrystallized from CH_2Cl_2/*n*-hexane at 0 °C to get pure compound (**1**) (0.375 g, 91%), mp 178 °C. Crystals suitable for single crystal X-ray diffraction were obtained after dissolving **1** in CH_2Cl_2/*n*-hexane and allowing it to remain at room temperature for two days. The molecular structure of **1** is given in Fig. 1. The supramolecular interactions present in this compound are summarized in Figure S1–S5. Table S1 provides the crystallographic and structure refinement data. FTIR (KBr) (ν/cm^{-1}): 3448 m, 3039s, 2923 m, 1615 s, 1591 s, 1316 s, 1181 s, 1061 s, 1036s, 837 s, 823 s, 714 s, 508 s, 480 s. ^{1}H NMR (400 MHz, $CDCl_3$, 25 °C, TMS) δ (ppm): 4.03 (s, 5*H*, Cp ring); 4.28 (s, 2*H*, two aromatic C*H*); 4.58 (s, 2*H*, two aromatic CH); 8.27 (s, 1*H*, imino); 7.92–8.24 (m, 9*H*-Pyrene, aromatic). ^{13}C NMR (100 MHz, $CDCl_3$, 25 °C, TMS) δ (ppm): 115.64, 123.26, 124.69, 124.97, 125.28, 125.59, 126.02, 126.21, 126.85, 127.35, 128.93, 131.57, 131.64, 147.10, 162.21. Anal. Calcd. for $C_{27}H_{20}FeN$; ESI-HRMS: $[\mathbf{1}+H]^+$ = Calculated 414.0945, found 414.0948; for $C_{54}H_{39}Fe_2N_2$; $[2(\mathbf{1})+H]^+$ = Calculated 827.1812, found 827.1757.

Results and Discussion

Crystal Structure

The compound **1** crystallized in monoclinic crystal system and *P*2(1)/c space group. It represents a Schiff base composed of one unit of each of the ferrocene and 1-Pyrenylamine (Fig. 1). The azomethine bond distance [C(11)-N(1)] is 1.282 Å, and the C(11)-N(1)-C(13) angle 120.55 ° which suggests co-planarity of -C=N- group with substituted cyclopentadinyl ring of ferrocene. The pyrenyl ring lies quite perpendicular to the ferrocenyl moiety which is evident by the pyrenyl ring plane intersecting the ferrocenyl moiety exactly through the half way in a vertical fashion (Figure S2). The centroid to centroid distance between ferrocenyl group and pyrenyl group is 7.770 Å which can be suited for donor (ferrocene)-acceptor (pyrene) energy transfer (vide supra). The molecule involves over thirteen C-H···π

interactions whereas lacks any π ··· π interactions despite the presence of highly planar pyrene group (Figure S3–S5).

UV–Visible and Fluorescence

The absorption spectra of **1** (Fig. 2a) was acquired in aqueous/acetonitrile (9:1, *v*/*v*); the low energy absorption maxima at 380 nm can be assigned to aromatic fluorophore π-π* transition [7–11]. Probing the interaction of **1** with various metal ions (Ca^{2+}, Cd^{2+}, Cu^{2+}, Li^{+}, Mg^{2+}, Mn^{2+}, Na^{+}, Ni^{2+}, Pb^{2+}, Zn^{2+}) resulted in the remarkable change in its absorption spectra only with Cu^{2+}. Emergence of a new broad band at ~500 nm is seen (Fig. 2a) which may probably be associated to the *d-d* transitions. Titrating **1** by adding increasing amount of Cu^{2+} leads to decrease in the band intensity at ~380 nm and successively a new band at 320 nm appears increasingly. Further, the isosbestic point is wavelength at which the total absorbance of a sample does not change during a chemical reaction between the two or more than two species. A clear isosbestic point observed at 350 nm suggests presence of more than two species (**1**, Cu^{2+} and **1**·Cu^{2+}) in the solution (Fig. 2b).

In addition, **1** shows strong dual emission bands with λ_{max} ~351 and ~420 nm, upon excitation at 326 nm. As noted in the absorption spectral studies, interaction of **1** with various metal salts reveals significant fluorescence change only with Cu^{2+} (Fig. 3a). To elaborate this highly selective change in fluorescence intensity, we further titrated **1** with increasing concentration of Cu^{2+} and observed strong quenching of the emission band associated with pyrene fluorophore. Addition of even 5 μM of Cu^{2+} causes considerable decrease in the intensity of the band at 420 nm (Fig. 3b).

Quantum yield (φ) for probe **1** calculated to be 0.067. The lower value of φ for **1** is attributed to the transfer of lone pair of electrons of the Schiff base nitrogen atom (-C=N-) to the conjugated pyrene ring via photo induced electron transfer (PET) mechanism [66]. Further, binding of **1** with Cu^{2+} decreases the φ value to 0.013. It is worth mentioning that the maximum extent of fluorescence quenching takes place to the band at 420 nm rather at 351 nm (although band at 351 nm also exhibits fluorescence quenching) (Fig. 3). It has been monitored that fluorescence behaviour of **1** at 420 nm do not affect in the presence of competing cations (a set of tested metal ions shown above). Interaction of **1** with Cu^{2+} was also probed in the background presence of competing metal ions by preliminary addition of various metal ions to the solution of **1** followed by addition of Cu^{2+}. The fluorescent spectral feature changes only with Cu^{2+} which strongly suggests the high selectivity of **1** toward fluorescent detection of Cu^{2+} even in the background presence of other metal ions (Figure S6). The binding constant of **1** with Cu^{2+} has been estimated to be 5.1×10^4 (lit mol^{-1}) from the fluorescence titration data considering a 1:1 binding mode as confirmed by the Job's plot (Figure S7). In general, in a

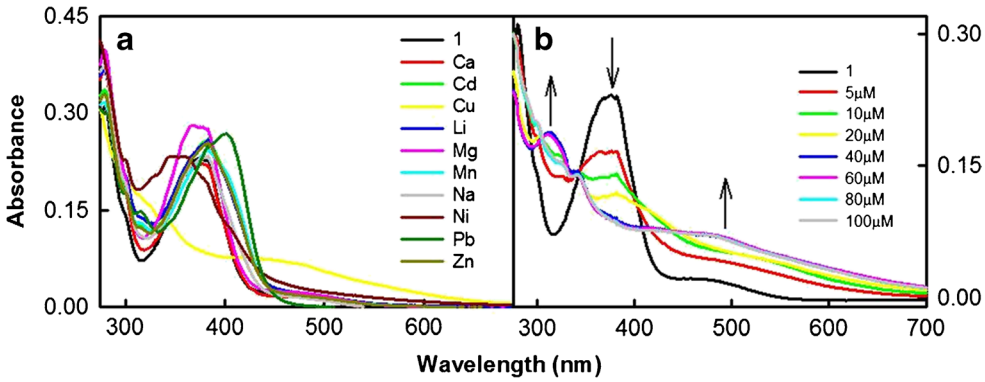

Fig. 2 **a** UV–visible spectra of **1** (H_2O/CH_3CN, 9:1, *v*/*v*, 10 μM) upon addition of 10 equiv of various metal ions. **b** UV–visible titration spectra of **1** upon addition of increasing amount (0–100 μM) of Cu^{2+}

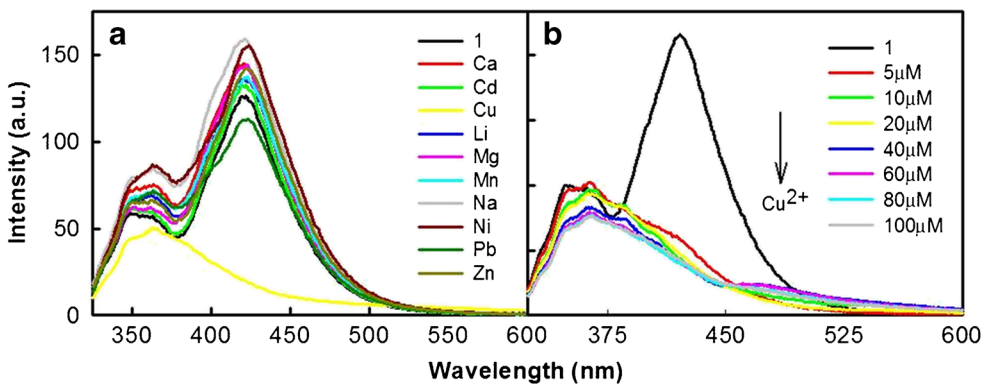

Fig. 3 **a** Fluorescence spectra of **1** (**a**) (H_2O/CH_3CN, 9:1, *v*/*v*, 10 μM) upon addition of 10 equiv of various metal ions. **b** Fluorescence spectra of **1** upon addition of increasing amount (0–100 μM) of Cu^{2+} ion

particular oxidation state, enthalpy of hydration and ionic radius decreases going from left to right amongst first row transition metal ion i.e. (M^{2+}). Further, Irving-William series states highest reactivity and binding strength of Cu(II) ion over other 3d metal ions. These factors promote Cu(II) ion as most preferred metal ion (a hard cation) for binding with hard donors like 'N' and 'O' in aqueous medium.

It is a tedious job to get exact distance between ferrocene-pyrene conjugate and Cu^{2+} without having crystal structure. However, as evident from literature, the bond distance between Cu^{2+} ion and monodentate N-donor ligand lies approximately in the range of 2.0–2.2 Å. Further, as evident from crystal structure, centroid to centroid distance between donor (ferrocene) and acceptor (pyrene) is 7.770 Å. Therefore, considering the entire crystal structure of **1**, bond length of N-C(pyrene) = 1.42, and N-Cu(II)~2.00-2.24 Å and the Ferrocene-N-Cu(II)/Pyrene-N-Cu(II) angles, the donor-Cu^{2+} distance should be in the range of 4.0–6.0 Å whereas acceptor- Cu^{2+} distance should be in the range of 5.5–7.5 Å. In addition, binding of Cu^{2+} through nitrogen of **1** will disturb the extended conjugation between donor and acceptor and may also change the donor–acceptor distance by geometrical distortion. Since Cu^{2+} is a paramagnetic ion thus it promotes ICT process upon binding with probe, responsible for fluorescence quenching.

Two Photon Absorption Cross Section

We have studied the two photon absorption (TPA) cross section of the compound **1**, but were unable to get any measurable TPA value. However, keeping in mind that the optimum fluorescence quenching was observed after addition of 10 equiv Cu^{2+} to the solution of **1** (referred as **2**), the TPA cross section change was monitored at this concentration and found 1230 GM.

Figure 4a shows the open aperture z-scan plot for the Cu-complex at a wavelength of 780 nm with the theoretical fit. We have also measured the TPA spectra of **2** in the wavelength range of 730–820 nm (Fig. 4b) and observed absorption maxima at 780 nm. TPA spectra of these both species follow similar trends as the single photon spectra of the respective complexes. We have also tried to measure the changes of TPA of **1** upon interaction with various cations used in the fluorescence study but no measurable TPA was observed.

We did not detect any two-photon induced fluorescence (TPIF) signal with reference to Rhodamine-6G within our wavelength tuning range of 730–820 nm. Re-absorption of emitted photons by itself, which is known as two photon absorption excited intramolecular energy transfer [67] may be the reason for the absence of TPIF in **2**. We cannot completely rule out the possibility of fluorescence quenching upon metal mediation in **1** as the cause of absence of TPIF in **2**.

DFT Calculations

Geometry optimization for **1** was carried out by DFT methods using GAUSSIAN 03 program as reported previously by us [43]. The optimized molecular geometry of **1** has C_1 symmetry, which is in good agreement with the one-photon spectra of 371 nm wavelength that result from the HOMO and LUMO energies of − 5.22 and − 1.87 eV, respectively. The HOMO and LUMO of **1** (Fig. 5) is delocalized across the whole molecular framework that is indicative of the lack of intramolecular charge transfer process thereby leaving no measurable TPA activity in it. The TPA cross-section in compound **1** became operative when its solution was treated with Cu^{2+} ions, which is probably due to an increased intramolecular charge transfer through the metal center. Experimental results reveal that the λ_{max} for TPA is in good agreement with OPA (one photon absorption) indicating resonant transition upon excitation.

Origin of TPA cross-section upon interaction of **1**with Cu^{2+} is probably due to the electron withdrawal by Cu^{2+} ion that results in the electron deficiency at the azomethine

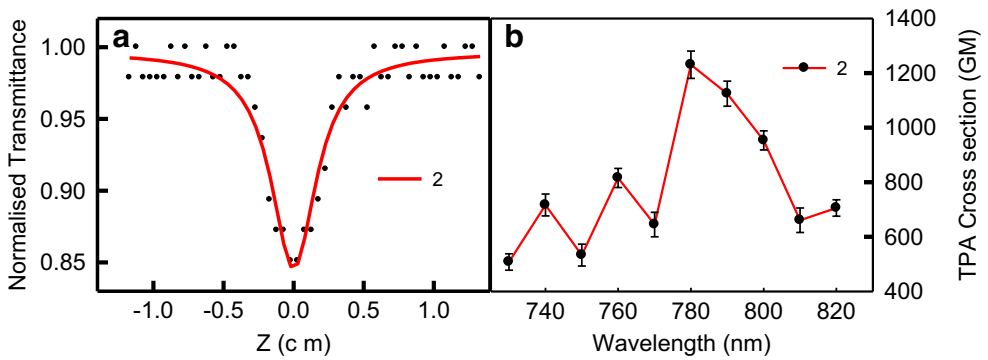

Fig. 4 **a** Open aperture z-scan of **2** (H_2O/CH_3CN, 9:1, *v*/*v*) at 780 nm. Solid lines are the best fitted of the experimental data. **b** Two photon spectra of **2** calculated using open aperture z-scan method

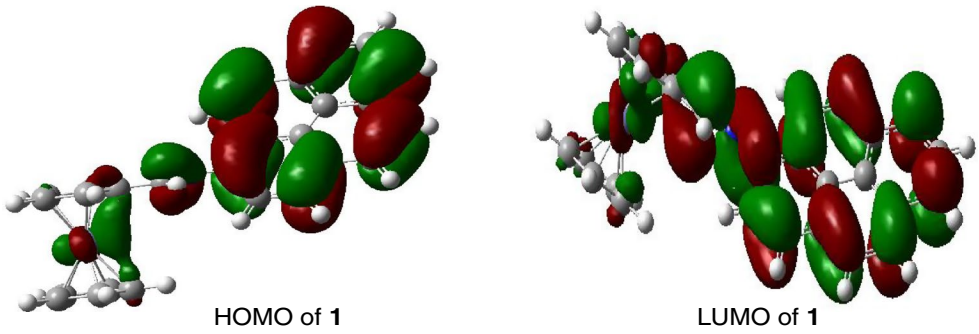

Fig. 5 Energy envelope plots for **1**

Scheme 1 Mechanism of two-photon absorption cross-section activity of ferrocenylated pyrene moieties

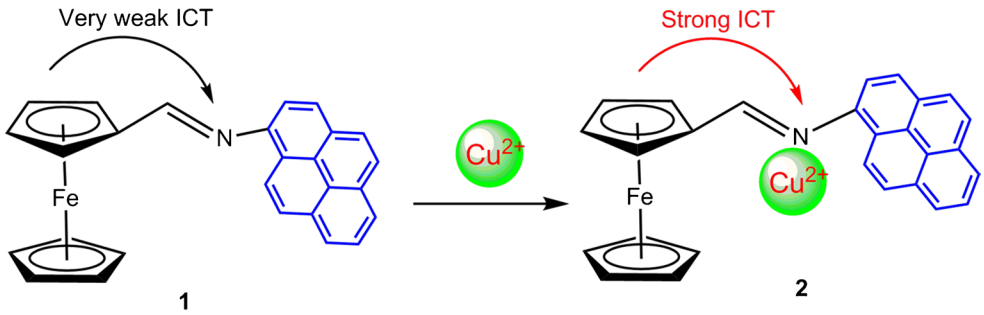

(-C=N-) nitrogen. The ferrocene moiety functions as an electron-donor which thus results in two D-π-A motifs. It is conjectured that the electron donating and accepting groups have the tendency to interact inter-molecularly in the ground state to result in the formation of charge-transfer complexes. The onset of TPA in **2** is due to the formation of charge-transfer complexes that favour the generation of third-order non linear optical behaviour (Scheme 1).

Electrochemical Studies

Cyclic voltammetric studies were performed in H_2O:CH_3CN (*v*/*v*; 9:1) using 10 μM concentration of the compound (**1**) and 0.1 M KCl as a supporting electrolyte. Notably, compound **1** displayed two irreversible oxidative waves at 0.39 and 0.80 V (vs Ag/AgCl) (Fig. 6). The wave at 0.80 V is attributed to the Fe^{2+}/Fe^{3+} redox couple, however the oxidative wave at lower potential (0.39 V) may be associated with the CH_3CN oxidation in mixed solvent media [44–46]. However, no reduction process was observed within the solvent cathodic potential limit. Such electrochemical behaviour is well known for ferrocene containing compounds [47–50].

Addition of Cu^{2+} (10 μM) led to the negative potential shift in both the oxidative waves to appear at 0.25 and 0.68 V (red line, Fig. 6). Further, additions of Cu^{2+} (20–100 μM) caused decrease in the current intensity and eventually both the oxidative waves disappeared. Consequently, it is clear

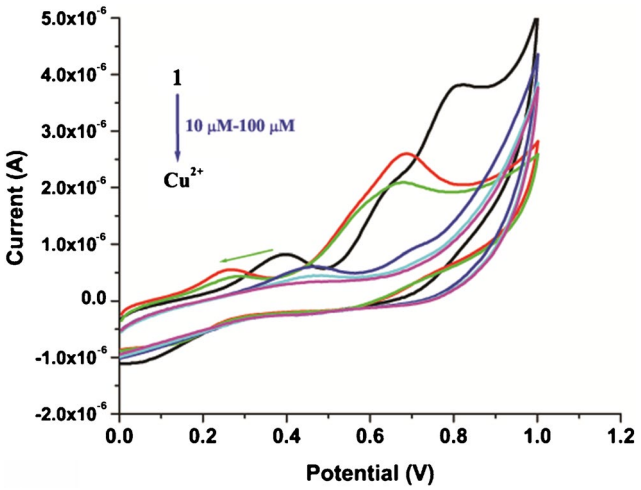

Fig. 6 Electrochemical titration plot of **1** (10 μM) in the presence of increasing Cu^{2+} amount in H_2O:CH_3CN (9:1)

that binding of Cu^{2+} occurs with **1** which can be evidently detected by electrochemical technique.

Conclusions

We have described a novel dual-signaling ferrocene-pyrene dyad that can selectively detect Cu(II) ions in presence of other metal ions. The first method of detection consists of

fluorescence quenching in the presence of copper (II) ions, while the second method involves an increase of TPA cross section upon metal binding. **1** exhibited Fe^{2+}/Fe^{3+} oxidative wave which upon addition of Cu(II) shifted toward negative potential that suggested the possible detection ability of **1** for Cu(II) ion through electrochemical technique.

Acknowledgements MAW is thankful to UGC for providing financial assistance and Department of Chemistry, Dr. H. S. Gour Central University Sagar, India, for providing the necessary facilities. MDP is thankful to UGC India for UGC-startup grant [F.No.30–56/2014(BSR)] and DST India for SERB research grant (EMR/2016/001779). RPP acknowledges DST for providing financial assistance through DST-Inspire Faculty scheme (IFA12-CH-66). SKM is thankful to UGC India for a fellowship. DG thanks the Welcome Trust International Senior Research Fellowship (UK) funds. We are thankful to Prof V Chandrasekhar and Prof Sandeep verma; IIT Kanpur for constant encouragement and support.

References

1. Carter KP, Young AM, Palmer AE (2014) Fluorescent sensors for measuring metal ions in living systems. Chem Rev 114:4564–4601
2. Yeunga MC-L, Yam VW-W (2015) Luminescent cation sensors: from host–guest chemistry, supramolecular chemistry to reaction-based mechanisms. Chem Soc Rev 44:4192–4202
3. Wani MA, Singh PK, Pandey R, Pandey MD (2016) Coumarin–pyrene conjugate: synthesis, structure and Cu-selective fluorescent sensing in mammalian kidney cells. J Lumin 171:159–165
4. Domaille DW, Zeng L, Chang CJ (2010) Visualizing ascorbate-triggered release of labile copper within living cells using a ratiometric fluorescent sensor. J Am Chem Soc 132:1194–1195
5. Tang R, Lei K, Chen K, Zhao H, Chen J (2011) A rhodamine-based off–on fluorescent chemosensor for selectively sensing Cu(II) in aqueous solution. J Fluoresc 21:141–148
6. Hsieh Y-C, Chir J-L, Yang S-T, Chen S-J, Hu C-H, Wu A-T (2011) A sugar-aza-crown ether-based fluorescent sensor for Cu2+ and Hg2+ ions. Carbohydr Res 346:978–981
7. Chandrasekhar V, Pandey MD (2011) Fluorescence sensing of Cu2+ and Hg2+ by a dipyrene ligand involving an excimer-switch off mechanism. Tetrahedron Lett 52:1938–1941
8. Chandrasekhar V, Pandey MD, Bag P, Pandey S (2009) A modular ligand design for cation sensors: phosphorus-supported pyrene-containing ligands as efficient Cu(II) and Mg(II) sensors. Tetrahedron 65:4540–4546
9. Pandey MD, Mishra AK, Chandrasekhar V, Verma S (2010) Silver-guided excimer emission in an Adenine-Pyrene conjugate: fluorescence lifetime and crystal studies. Inorg Chem 49:2020–2022
10. Chandrasekhar V, Bag P, Pandey MD (2009) Phosphorus-supported multidentate coumarin-containing fluorescence sensors for Cu2+. Tetrahedron 65:9876–9883
11. Faggi E, Serra-Vinardell J, Pandey MD, Casa J, Fabriàs G, Luis SV, Alfonso I (2016) Pseudopeptidic fluorescent on-off pH sensor based on pyrene excimer emission: imaging of acidic cellular organelles. Sensors Actuators B 234:633–640
12. Gaggelli E, Kozlowski H, Valensin D, Valensin G (2006) Copper homeostasis and neurodegenerative disorders (Alzheimer's, prion, and Parkinson's diseases and amyotrophic lateral sclerosis). Chem Rev 106:1995
13. Khatua S, Choi SH, Lee J, Huh JO, Do Y, Churchill DG (2009) Highly selective fluorescence detection of Cu2+ in water by chiral dimeric Zn2+ complexes through direct displacement. Inorg Chem 48:1799
14. Yan S, Leen V, Snick SV, Boens N, Dehaen W (2010) A highly sensitive, selective, colorimetric and near-infrared fluorescent turn-on chemosensor for Cu2+ based on BODIPY. Chem Commun 46:6329
15. Jung HS, Park M, Han DY, Kim E, Lee C, Ham S, Kim JS (2009) Cu2+ ion-induced self-assembly of pyrenylquinoline with a pyrenyl excimer formation. Org Lett 11:3378
16. Jung HS, Kwon PS, Lee JW, Kim JI, Hong CS, Kim JW, Yan SH, Lee JY, Lee JH, Joo TH, Kim JS (2009) Coumarin-derived Cu2+-selective fluorescence sensor: synthesis, mechanisms, and applications in living cells. J Am Chem Soc 131:2008
17. Chandrasekhar V, Das S, Yadav R, Hossain S, Parihar R, Subramaniam G, Sen P (2012) Novel chemosensor for the visual detection of copper(II) in aqueous solution at the ppm level. Inorg Chem 51:8664
18. Carpentieri U, Myers J, Thorpe L, Daeschner CW III, Haggard ME (1986) Copper, zinc, and iron in normal and leukemic lymphocytes from children. Cancer Res 46:981
19. Halfdanarson TR, Kumar N, Li CY, Phyliky RL, Hogan WJ (2008) Hematological manifestations of copper deficiency: a retrospective review. Eur J Haematol 80:523
20. Jaiser SR, Winston GP (2010) Copper deficiency myelopathy. J Neurol 257:869
21. Moghaddam MM, Pirouzi M, Saberi MR, Chamani J (2014) Comparison of the binding behavior of FCCP with HSA and HTF as determined by spectroscopic and molecular modeling techniques. Luminescence 29:314–331
22. Chamani J (2010) Energetic domains analysis of bovine α-lactalbumin upon interaction with copper and dodecyl trimethylammonium bromide. J Mol Struct 979:227–234
23. Bakaeean B, Kabiri M, Iranfar H, Saberi MR, Chamani J (2012) Binding effect of common ions to human serum albumin in the presence of norfloxacin: investigation with spectroscopic and zeta potential approaches. J Sol Chem 41:1777–1801
24. Kabiri M, Chamani J (2012) Study of the ropinirole hydrochloride interactions with human holo-transferrin in the presence of common metal ions. J Iran Chem Soc 9:625–633
25. He GS, Tan L-S, Zheng Q, Prasad PN (2008) Multiphoton absorbing materials: molecular designs, characterizations, and applications. Chem Rev 108:1245–1330
26. Pawlicki M, Collins HA, Denning RG, Anderson HL (2009) Two-photon absorption and the design of two-photon dyes. Angew Chem Int Ed 48:3244–3266
27. Albota M, Beljonne D, Bredas J-L, Ehrlich JE, Fu J-Y, Heikal AA, Hess SE, Kogej T, Levin MD, Marder SR, McCord-Maughon D, Perry W, Rockel JH, Rumi M, Subramaniam G, Webb WW, Wu XL, Xu C (1998) Design of organic molecules with large two-photon absorption cross sections. Science 281:1653–1656
28. Cai Z, Deng L, Zhou M, Gao J, Sun Z (2010) Third-order nonlinear optical studies of new anthraquinone derivatives. Opt Commun 283:5199–5202
29. Jana A, Lim JM, Park SW, Kim D, Bharadwaj PK (2011) A comparative study of third order optical nonlinearity of symmetrical dipolar chromogenic probes and their enhancement by different metal ions. Ind J Chem A 50A:511–518
30. Jana A, Jang SY, Shin J-Y, De AK, Goswami D, Kim D, Bharadwaj PK (2008) Attachment of different donor groups to a cryptand for modulation of two-photon absorption cross-section. Chem Eur J 14:10628–10638
31. Lee SK, Yang WS, Choi JJ, Kim CH, Jeon SJ, Cho BR (2005) 2,6-Bis[4-(p-dihexylaminostyryl)styryl]anthracene derivatives with large two-photon cross sections. Org Lett 7:323–326

32. Abbotto A, Beverina L, Bozio R, Facchetti A, Ferrante C, Pagani GA, Pedron D, Signorini R (2002) Novel heterocycle-based two-photon absorbing dyes. Org Lett 4:1495–1498
33. Wei P, Bi X, Wu Z (2005) Synthesis of triphenylamine-cored dendritic two-photon absorbing chromophores. Org Lett 7:3199–3202
34. Padilha LA, Webster S, Przhonska OV, Hu H, Peceli D, Ensley TR, Bondar MV, Gerasov AO, Kovtun YP, Shandura MP, Kachkovski AD, Hagan DJ, VanStryland EW (2010) Efficient two-photon absorbing acceptor-π-acceptor polymethine dyes. J Phys Chem A 114:6493–6501
35. Shao P, Huang Z, Li J, Chen S, Luo J, Qin J, Liu B (2006) Two-photon absorption properties of two (dicyanomethylene)-pyran derivatives. Opt Mat 29:337–341
36. Misra R, Kumar R, Chandrashekar TK, Suresh CH, Nag A, Goswami D (2006) 22π Smaragdyrin molecular conjugates with aromatic Phenylacetylenes and Ferrocenes: syntheses, electrochemical, and photonic properties. J Am Chem Soc 128:16083–16091
37. Kim HM, Lee YO, Lim CS, Kim JS, Cho BR (2008) Two-photon absorption properties of alkynyl-conjugated pyrene derivatives. J Org Chem 73:5127–5130
38. Rumi M, Barlow S, Wang J, Perry JW, Marder SR (2008) Two-photon absorbing materials and two-photon-induced chemistry. Adv Polym Sci 213:1–95
39. Hu J-Y, Era M, Elsegood MRJ, Yamato T (2010) Synthesis and photophysical properties of pyrene-based light-emitting monomers: highly pure-blue-fluorescent, cruciform-shaped architectures. Eur J Org Chem 2010:72–79
40. Bhaskar A, Ramakrishna G, Twieg RJ, Goodson T III (2007) Zinc sensing via enhancement of two-photon excited fluorescence. J Phys Chem C 111:14607–14611
41. Tian Y, Chen C-Y, Yang C-C, Young AC, Jang S-H, Chen W-C, Jen AK-Y (2008) 2-(2′-Hydroxyphenyl)benzoxazole-containing two-photon-absorbing chromophores as sensors for zinc and hydroxide ions. Chem Mater 20:1977–1987
42. Shi Z, Han Q, Yang L, Yang H, Tang X, Dou W, Li Z, Zhang Y, Shao Y, Guan L, Liu W (2015) A highly selective two-photon fluorescent probe for detection of cadmium(II) based on intramolecular electron transfer and its imaging in living cells. Chem Eur J 21:290–297
43. Chandrasekhar V, Azhakar R, Murgesapandian B, Senapati T, Bag P, Pandey MD, Maurya SK, Goswami D (2010) Synthesis, structure, and two-photon absorption studies of a phosphorus-based tris hydrazone ligand (S)P[N(Me)NdCH-C6H3-2-OH-4-N(CH2CH3)2]3 and its metal complexes. Inorg Chem 49:4008–4016
44. Chandrasekhar V, Pandey MD, Maurya SK, Sen P, Goswami D (2011) Two-photon absorption technique for selective detection of Copper(II) ions in aqueous solutions using a Dansyl-pyrene conjugate. Chem Asian J 6:2246–2250
45. Zhang P, Pei L, Chen Y, Xu W, Lin Q, Wang J, Wu J, Shen Y, Ji L, Chao Y (2013) A dinuclear ruthenium(II) complex as a one- and two-photon luminescent probe for biological Cu2+ detection. Chem Eur J 19:15494–15503
46. Lai RY, Fleming JJ, Merner BL, Vermeij RJ, Bodwell GJ, Bard AJ (2004) Electrogenerated chemiluminescence. 74. Photophysical, electrochemical, and electrogenerated chemiluminescent studies of selected nonplanar pyrenophanes. J Phys Chem A 108:376–383
47. Padamati SK, Draksharapu A, Unjaroen D, Browne WR (2016) Conflicting role of water in the activation of H_2O_2 and the formation and reactivity of non-heme FeIII–OOH and FeIII–O–FeIII complexes at room temperature. Inorg Chem 55:4211–4222
48. Pandey MD, Martí-Centelles V, Burguete MI, Montoya N, Luis SV, García-España E, Doménech-Carbó A (2016) Bisferrocenyl-functionalized pseudopeptides: access to separated ionic and electronic contributions for electrochemical anion sensing. RSC Adv 6:35257–35266
49. Zapata F, Caballero A, Espinosa A, Tárraga A, Molina P (2007) A simple but effective ferrocene derivative as a redox, colorimetric, and fluorescent receptor for highly selective recognition of Zn2+ ions. Org Lett 9:2385–2388
50. Kulhnek J, Bures F, Kuznik W, Kityk IV, Mikysek T, Ruzicka A (2013) Ferrocene-donor and 4,5-dicyanoimidazole-acceptor moieties in charge- transfer chromophores with π linkers tailored for second-order nonlinear optics. Chem Asian J 8:465–475
51. Kaur M, Kaur P, Dhuna V, Singh S, Singh K (2014) A ferrocene–pyrene based 'turn-on' chemodosimeter for Cr3+ – application in bioimaging. Dalton Trans 43:5707–5712
52. Keli Z, Baofeng G, Xue Z, Kedi C, Lijun T, Longyi J (2015) Ionics fluorescent chemsensor based on pyrene. Prog Chem 27:1230–1239
53. Chang X, Wang G, Yu C, Wang Y, He M, Fan J, Fang Y (2015) Studies on the photochemical stabilities of some fluorescent films based on pyrene and pyrenyl derivatives. J Photochem Photobiol A Chem 298:9–16
54. Venkatesan P, Wu S-P (2015) A turn-on fluorescent pyrene-based chemosensor for Cu(II) with live cell application. RSC Adv 5:42591–42596
55. Wu Y-S, Li C-Y, Li Y-F, Li D, Li Z (2016) Development of a simple pyrene-based ratiometric fluorescent chemosensor for copper ion in living cells. Sensors Actuators B 222:1226–1232
56. Dawson WR, Windsor MW (1968) Fluorescence yields of aromatic compounds. J Phys Chem 72:3251–3260
57. Bag B, Bharadwaj PK (2005) Perturbation of the PET process in fluorophore-spacer-receptor systems through structural modification: transition metal induced fluorescence enhancement and selectivity. J Phys Chem B 109:4377–4390
58. Sen P, Roy D, Mondal SK, Sahu K, Ghosh S, Bhattacharyya K (2005) Fluorescence anisotropy decay and solvation dynamics in a nanocavity: coumarin 153 in methyl â-Cyclodextrins. J Phys Chem A 109:9716–9722
59. Fujimoto K, Shimizu H, Inouye M (2004) Unambiguous detection of target DNAs by excimer-monomer switching molecular beacons. J Org Chem 69:3271–3275
60. Sheik-Bahae M, Said AA, Wei T, Hagan DJ, Van Stryland EW (1990) Sensitive measurement of optical nonlinearities using a single beam. IEEE J Quantum Electron 26:760–769
61. Das S, Nag A, Goswami D, Bharadwaj PK (2006) Zinc(II)- and copper(I)-mediated large two-photon absorption cross sections in a bis-cinnamaldiminato Schiff base. J Am Chem Soc 128:402–403
62. Nag A, De AK, Goswami D (2009) Two-photon cross-section measurements using an optical chopper: z-scan and two-photon fluorescence schemes. J Phys B: At Mol Opt Phys 42:065103
63. Fitilis I, Fakis M, Polyzos I, Giannetas V, Persephonis P, Vellis P, Mikroyannidis J (2007) A two-photon absorption study of fluorene and carbazole derivatives. The role of the central core and the solvent polarity. Chem Phys Lett 447:300–304
64. Sengupta P, Balaji J, Banerjee S, Philip R, Ravindra Kumar G, Maiti SJ (2000) Sensitive measurement of absolute two-photon absorption cross sections. J Chem Phys 112:9201
65. Tian P, Warren WS (2002) Ultrafast measurement of two-photon absorption by loss modulation. Opt Lett 27:1634
66. Brauge L, Vériot G, Franc G, Deloncle R, Caminade A-M, Majoral J-P (2006) Synthesis of phosphorus dendrimers bearing chromophoric end groups: toward organic blue light-emitting diodes. Tetrahedron 62:11891–11899
67. Oar MA, Dichtel WR, Serin JM, Frechet J, Rogers MJ, Slagle JEJE, Fleitz PA, Tan L-S, Ohulchanskyy TY, Prasad PN (2006) Light-harvesting chromophores with metalated porphyrin cores for tuned photosensitization of singlet oxygen via two-photon excited FRET. Chem Mater 18:3682–3692